University of Kentucky
UKnowledge

Chemistry Faculty Publications   Chemistry

5-1-2015

BH₂ Revisited: New, Extensive Measurements of Laser-Induced Fluorescence Transitions and *Ab Initio* Calculations of Near-Spectroscopic Accuracy

Fumie X. Sunahori
Franklin College

Mohammed Gharaibeh
University of Jordan, Jordan

Dennis J. Clouthier
University of Kentucky, dclaser@uky.edu

Riccardo Tarroni
Università di Bologna, Italy

Right click to open a feedback form in a new tab to let us know how this document benefits you.

Follow this and additional works at: https://uknowledge.uky.edu/chemistry_facpub

Part of the Chemistry Commons

Repository Citation

BH$_2$ Revisited: New, Extensive Measurements of Laser-Induced Fluorescence Transitions and *Ab Initio* Calculations of Near-Spectroscopic Accuracy

BH$_2$ revisited: New, extensive measurements of laser-induced fluorescence transitions and *ab initio* calculations of near-spectroscopic accuracy

Fumie X. Sunahori,[1] Mohammed Gharaibeh,[2] Dennis J. Clouthier,[3,a)] and Riccardo Tarroni[4]

[1]*Department of Chemistry and Physics, Franklin College, Franklin, Indiana 46131, USA*
[2]*Department of Chemistry, The University of Jordan, Amman 11942, Jordan*
[3]*Department of Chemistry, University of Kentucky, Lexington, Kentucky 40506-0055, USA*
[4]*Dipartimento di Chimica Industriale "Toso Montanari," Università di Bologna, Viale Risorgimento 4, 40136 Bologna, Italy*

The spectroscopy of gas phase BH$_2$ has not been explored experimentally since the pioneering study of Herzberg and Johns in 1967. In the present work, laser-induced fluorescence (LIF) spectra of the $\tilde{A}$ $^2B_1(\Pi_u) - \tilde{X}$ $^2A_1$ band system of ^{11}BH$_2$, ^{10}BH$_2$, ^{11}BD$_2$, and ^{10}BD$_2$ have been observed for the first time. The free radicals were "synthesized" by an electric discharge through a precursor mixture of 0.5% diborane (B$_2$H$_6$ or B$_2$D$_6$) in high pressure argon at the exit of a pulsed valve. A total of 67 LIF bands have been measured and rotationally analyzed, 62 of them previously unobserved. These include transitions to a wide variety of excited state bending levels, to several stretch-bend combination levels, and to three ground state levels which gain intensity through Renner-Teller coupling to nearby excited state levels. As an aid to vibronic assignment of the spectra, very high level hybrid *ab initio* potential energy surfaces were built starting from the coupled cluster singles and doubles with perturbative triples (CCSD(T))/aug-cc-pV5Z level of theory for this seven-electron system. In an effort to obtain the highest possible accuracy, the potentials were corrected for core correlation, extrapolation to the complete basis set limit, electron correlation beyond CCSD(T), and diagonal Born-Oppenheimer effects. The spin-rovibronic states of the various isotopologues of BH$_2$ were calculated for energies up to 22 000 cm^{-1} above the $\tilde{X}$ (000) level without any empirical adjustment of the potentials or fitting to experimental data. The agreement with the new LIF data is excellent, approaching near-spectroscopic accuracy (a few cm^{-1}) and has allowed us to understand the complicated spin-rovibronic energy level structure even in the region of strong Renner-Teller resonances. © *2015 AIP Publishing LLC.* [http://dx.doi.org/10.1063/1.4919094]

I. INTRODUCTION

Small boron-containing free radicals are intermediates in a variety of real-world applications, including the chemical vapor deposition (CVD) production of boron carbide[1] and boron nitride,[2] doping of semiconductors,[3] plasma etching and reactive ion etching of circuit elements,[4] the production of boron-containing films,[5] and the incorporation of boron in steel,[6] to name just a few. It is, therefore, important to establish sensitive methods for detecting and characterizing such reactive species to aid in experimental and theoretical programs aimed at optimizing the industrial processes. Such methods are most likely to be spectroscopic in nature, and future studies of the transient intermediates involved will rely on a well-established database of molecular constants, transition frequencies, and molecular structures. In recent years, we have been engaged in spectroscopic studies of boron species in the gas phase, a program which has yielded considerable new information[7–14] on the BS$_2$, HBF, HBCl, HBBr, BF$_2$, and F$_2$BO free radicals. In the present work, we

turn our attention to BH$_2$, a fundamental species for which there is a dearth of information.

The first and only spectroscopic study of the BH$_2$ free radical in the gas phase was reported by Herzberg and Johns[15] in 1967. A new absorption spectrum in the 640-870 nm region was found in the flash photolysis of borane carbonyl (H$_3$BCO). The widely spaced rotational fine structure, the marked rotational line intensity alternation, the boron isotope effects, and the vibrational and rotational changes on deuterium substitution all firmly established the carrier of these bands as the BH$_2$ free radical. BH$_2$ is bent in the ground state and linear in the excited state, and the observed electronic transition is between the two components of what would be a $^2\Pi$ state at linearity. It is rather remarkable that in the intervening almost half a century, no further experimental spectroscopic studies of this interesting gas phase species have been reported. Although the ESR spectrum of BH$_2$ in a neon matrix has been obtained,[16] the microwave and infrared spectra are unknown, and the electronic spectroscopy has not been further explored.

Despite the dearth of experimental attention, BH$_2$, with only seven electrons, has been fertile ground for a large variety of theoretical studies, too numerous to discuss in detail here. Of particular relevance to the present work are

a)Author to whom correspondence should be addressed. Electronic mail: dclaser@uky.edu

142, 174302-1

ab initio studies of the ground and first excited state rovibronic energy levels[17–19] culminating in a very detailed calculation[19] including the effect of the electronic angular momentum and spin-orbit coupling. These calculations have been used to correct the vibrational assignments of the bands observed by Herzberg and Johns,[15] to predict that $T_0 = 4203.9$ cm^{-1} for ^{11}BH$_2$, and to obtain the ground and excited state r_e structures as $r'' = 1.1875$ Å, $\theta'' = 129.04°$, $r' = 1.1698$ Å, and $\theta' = 180°$.

In addition to these fundamental spectroscopic and theoretical studies, there have been concerted efforts to understand the importance of BH$_2$ in industrial processes. Several theoretical studies[20–25] have examined aspects of the thermodynamics, reaction pathways, intermediates and transition states in diborane degradation in CVD, boron carbide production, and boron nitride growth processes. In 1989, Atkinson and coworkers[26] reported using intracavity absorption spectroscopy *in situ* to detect BH$_2$ during the plasma dissociation of diborane, under conditions similar to those employed industrially in the deposition of boron films. Their study established, for the first time, the presence of the BH$_2$ reactive intermediate under CVD conditions and highlighted its importance in such reactions.

II. EXPERIMENT

The BH$_2$ and BD$_2$ free radicals were produced in a discharge free jet expansion[27] using precursor mixtures of 0.5% diborane (B$_2$H$_6$) or fully deuterated diborane (B$_2$D$_6$) in high pressure argon. The gas mixture was injected at a pressure of 30–40 psi through the 0.8 mm orifice of a pulsed molecular beam valve (General Valve, Series 9) into the vacuum chamber. After a short time delay, a pulsed electric discharge was struck between a pair of ring electrodes mounted in a cylindrical Delrin flow channel attached to the exit to the valve, fragmenting the precursors and producing BH$_2$ in the process. The radicals were cooled to low rotational temperatures ($\sim$10 K) by collisions downstream of the discharge. A 1.0 cm long, 4 mm inner diameter reheat tube[28] was attached to the exit of the discharge flow channel to increase the number of collisions which both enhanced the production of the radicals and suppressed the background glow from electronically excited argon atoms.

Low-resolution laser-induced fluorescence (LIF) spectra were recorded by exciting the jet-cooled radicals with the collimated beam of a pulsed tunable dye laser (Lumonics HD-500, linewidth 0.1 cm^{-1}) and imaging the resulting fluorescence signals onto the photocathode of a high gain photomultiplier (EMI 9816QB). The signals were sampled with a gated integrator and recorded with LabVIEW–based data acquisition software. The spectra were calibrated with optogalvanic lines from neon- and argon-filled hollow cathode lamps to an accuracy of $\sim$0.1 cm^{-1}.

The LIF spectra of ^{10}BH$_2$ and ^{10}BD$_2$ were often overlapped by bands of the stronger ^{11}B isotopologues. To circumvent these problems, we used the LIF synchronous scanning (sync-scan) technique described previously.[14] In this method, the fluorescence is dispersed by a scanning monochromator which is fixed on a prominent emission band

of the isotopologue(s) of interest. The excitation laser and the monochromator are scanned synchronously under computer control so that the resulting spectrum exhibits only those transitions that emit down to the chosen level, focusing on the spectrum of a subset of the molecular isotopologues and minimizing impurity emission.

High resolution sync-scan LIF spectra were obtained in the same fashion but using a dye laser equipped with an intra-cavity angle-tuned etalon (Scanmate 2E), providing tunable radiation with a linewidth of 0.035 cm^{-1}. All high resolution spectra were calibrated with iodine LIF transitions.[29]

Diborane (B$_2$H$_6$) and fully deuterated diborane (B$_2$D$_6$) were synthesized by the reaction of sodium borohydride (NaBH$_4$ or NaBD$_4$) with phosphoric acid (H$_3$PO$_4$ or D$_3$PO$_4$) using the standard literature method.[30]

III. EXPERIMENTAL RESULTS AND ANALYSIS

A. Preliminary considerations

As originally shown by Herzberg and Johns,[15] BH$_2$ is a bent near-prolate asymmetric top in the ground state, and the first electronic transition is ^{2}B$_1$(Π_u) $-$ ^{2}A$_1$, which follows *c*-type rotational selection rules. The presence of two equivalent hydrogen nuclei necessitates a 3:1 [eo, oe:ee,oo] (BD$_2$ =2:1 [ee,oo:eo,oe]) nuclear statistical weight alternation in the populations of the lower state levels of BH$_2$. We label the energy levels of both states by the asymmetric top quantum numbers $N_{K_aK_c}$ in the absence of resolvable electron spin splittings. In the upper linear state, K'_a designates the value of l' while the two values of K'_c distinguish the *l*-type doubling components. In those instances where the spin splittings are resolved, the rotational levels are designated by J, the quantum number for the total rotational plus spin angular momentum: $J = N + 1/2$(F$_1$) and $J = N - 1/2$(F$_2$). The vibrations of BH$_2$ are labeled ν_1(a$_1$) = BH symmetric stretch, ν_2(a$_1$) = bend, and ν_3(b$_2$) BH antisymmetric stretch.

Fig. 1 shows a schematic correlation diagram between the energy levels of the linear excited state and the bent ground state of BH$_2$. Starting from the left hand side of Fig. 1, the energy levels of a linear molecule in a $^1\Pi$ state with vibronic angular momentum quantum number $K = |\pm\Lambda \pm l|$ are represented. The inclusion of non-zero spin-orbit coupling further splits the vibronic levels of a $^2\Pi$ state into levels labeled by the term symbols $^{2S+1}K_P$, where $P = |\pm\Omega \pm l| = |\pm K \pm \Sigma|$. In the BH$_2$ case, bending of the molecular frame splits the degenerate $^2\Pi$ potential into two components, an upper one with a single minimum at 180° and a lower double minimum potential with an equilibrium HBH angle near 129°. The right hand side of Fig. 1 shows the energy levels for the excited linear state (upper panel) and the bent ground state (lower panel) and their correlations with the energy levels of the linear $^2\Pi$ state.[31] It is found that for each group of linear Π state vibronic levels with the same bending vibrational quantum number, the uppermost levels with $K \leq v_2 - 1$ correlate with vibronic levels of the linear excited state, while the other vibronic levels correlate with vibrational and rotational levels of the bent ^{2}A$_1$ ground state. It is apparent from Fig. 1 that the $v_2 = 0$ ($K = 1$) levels of the linear molecule correlate with
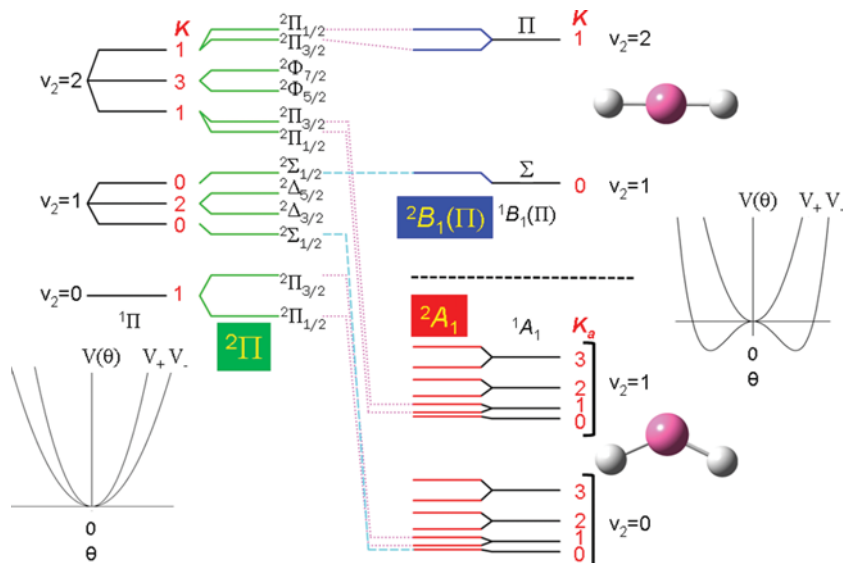
FIG. 1. Schematic diagram of the bending levels of an AB_2 triatomic molecule. The left hand side depicts the energy levels of a molecule in a $^1\Pi$ or $^2\Pi$ state in the limit of small vibronic interaction. The right hand side depicts the corresponding energy levels of a molecule with a large vibronic interaction, such that the lower potential curve has a minimum at a nonlinear geometry. The correlation between the energy levels in the strictly linear and linear/bent cases is given.

the $v_2 = 0$, $K_a = 1$ levels of the bent $^2A_1$ state. As a result, the upper (linear) state does not have a $v_2 = 0$ level, but rather commences with a $v_2 = 1$, $K = 0$, Σ level, and there is an alternation with the $v_2 =$ odd levels having Σ, Δ, ... symmetry ($K =$ even values) and $v_2 =$ even levels having Π, Φ, ... symmetry ($K =$ odd values). We denote the lower state bending levels by the v_2 quantum number appropriate for the bent molecule and the upper state levels by the v_2 appropriate for a linear molecule.[19]

In a $^1A_1$ ground state, the bending levels ($v_2 = 0, 1, 2, ...$) have the rotational levels of an asymmetric top, labeled by J_{KaKc}, although only the K_a stacks are shown in Fig. 1. A single unpaired electron generates a $^2A_1$ state whose rotational energy levels exhibit further spin splittings.

B. Medium resolution LIF spectra

Relatively intense LIF spectra of BH_2 and BD_2 were readily obtained in the 12 500–22 000 cm^{-1} region as shown in Fig. 2. Our spectrum of BH_2 extends some 5500 cm^{-1} to higher wavenumbers of that reported by Herzberg and Johns,[15] and

the present spectra of BD_2 are new information. In each case, the major progression of bands is readily identified, based on the calculated band positions given by Kolbuszewski *et al.*,[19] modified as necessary by our own calculations (see Sec. IV), as the bending progression, and extending from $v_2' = 10$ to 19 in $^{11}BH_2$ and $v_2' = 14$ to 23 in $^{11}BD_2$. As primarily $K_a'' = 0$ and 1 BH_2 levels are populated in our supersonic expansion (in some cases we also see weaker transitions from $K_a'' = 2$), the $\Delta K_a = \pm1$ selection rule necessitates that the transitions terminate on $K' = 1$ or Π levels for $v_2' =$ even and $K' = 0$ or 2 (Σ or Δ) levels for $v_2' =$ odd, leading to the Π, Σ band alternation observed in the spectrum and proven by rotational analysis (*vide infra*). The BH_2–BD_2 vibronic band isotope effects are very large (~3300 cm^{-1} for the transitions to the $v_2' = 14$ Π bands—see Fig. 2). In most cases, weaker ^{10}B isotopologue bands were identifiable 50-150 cm^{-1} to higher wavenumbers of the stronger features as illustrated in Fig. 3. In addition, other weaker bands were vibronically assigned as transitions to excited state bend-stretch combination levels and to mixed ground/excited state levels based on the results of our theoretical calculations (see Secs. IV and V).
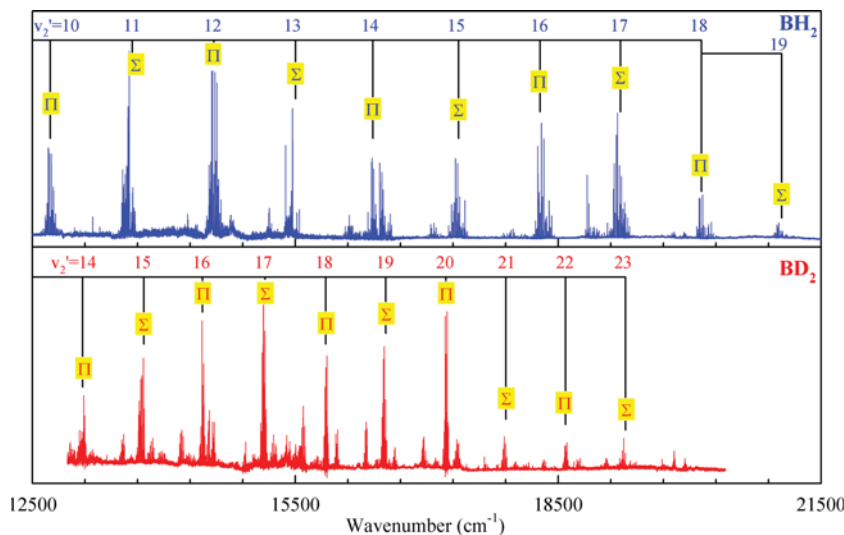

FIG. 2. Composite medium resolution LIF spectra of BH_2 and BD_2. These spectra were constructed by piecing together multiple scans over several laser dye regions so the relative intensities of the various bands are not very meaningful. The major bending progression 2_0^n is identified in each case.
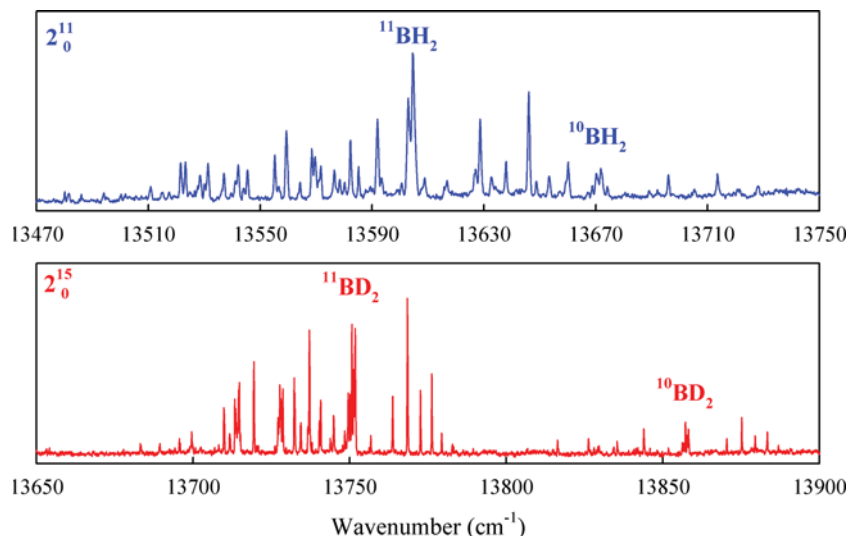
FIG. 3. Two medium resolution bands showing the ^{11}B–^{10}B isotope shifts in the spectra of BH$_2$ and BD$_2$. In each case, the central Q-branch of the particular isotopologue is identified.

As an example of the rotational analysis of the bands, we show in Fig. 4 the LIF spectrum of the 2_0^{10} band of ^{11}BH$_2$, illustrating the well-resolved rotational structure at modest resolution (0.1 cm^{-1}) and some of the rotational assignments. The 2_0^{10} band involves the transition from $K'' = 0$ to $K' = 1$ and is therefore a Π type band and clearly exhibits the expected intensity alternation due to the lower state nuclear statistical weights. Although the corresponding $K'' = 2$ to $K' = 1$ subband might also be expected at lower wavenumbers, no trace of it was found, due to the weakness of the main subband and the effective cooling in the supersonic expansion. [These weaker subbands were found in some cases for the stronger vibronic transitions and they are very useful for making further ground state combination differences (GSCDs).] The $^rR_0$ branch lines are readily apparent at the blue end of the band and were assigned based on the regular pattern of transitions and intensity alternations. The $^rP_0$ lines were then readily located using $^rR_0(N'') - {}^rP_0(N'' + 2)$ GSCDs [both sets of lines terminate on the same N'_{KaKc} level in the upper state] in comparison to those derived from Table III of Ref. 15. Since the Q-branch lines terminate on the opposite asymmetry component in the excited state [for example, $^rR_0(1)$ is 2_{11}-1_{01} (N_{KaKc}), whereas $^rQ_0(2)$ is 2_{12}-2_{02}], it was not

possible to form GSCDs with the P- or R-branch lines, so assignments were made based largely on intensities and the expected pattern of lines. No spin splittings are evident in any of the lines in this particular band at this resolution.

For examples of Σ and Δ bands, we show in Fig. 5 the 2_0^{15} spectrum of ^{11}BD$_2$. The Σ band involves a $K' = 0 - K'' = 1$ transition, while the Δ band originates in the same lower state K stack but terminates in the $K = 2$ (Δ) component of the $\tilde{A}(0, 15, 0)$ vibrational state. The most obvious features of the Σ band are the well-resolved $^PR_1$ branch and the corresponding very compact Q-branch. Comparison of the R-branch lines of a Σ band and a Π band (Fig. 4) shows two diagnostic differences. In the Σ band, the separation of the first lines of the R- and Q-branches is large, approximately $4B'$ [for ^{11}BD$_2$ (0,15,0), this is $\sim$12 cm^{-1}], as the two terminate on the $N' = 1$ and $N' = 2$ levels. In a Π band of ^{11}BD$_2$ (not shown), this separation is the difference between the $K''_a = 0$, $N'' = 0$ and $N'' = 1$ levels, approximately $B'' + C''$, which for the (0,16,0) ^{11}BD$_2$ Π band is $\sim$5.5 cm^{-1}, about half that of the neighboring Σ band. Second, in a given isotopologue, the pattern of R-branch intensity alternation is different. In BH$_2$, the first Π band R-branch line is weak (lower level = $0_{0,0}$ or ee) and the first Σ band line is strong (lower level = $1_{1,0}$ or oe). The situation is exactly reversed in BD$_2$. The analysis of the Σ bands proceeded much the same as that of the Π bands described above. Since the energy level separations are known for the ground state, and there are no asymmetry splittings in the $K = 0$ upper state, in this case, it was possible to form ground state combination differences for all three branches.

The upper state bending levels shown in Fig. 1 are the simplest cases at very low values of v$_2'$. For higher levels with odd v$_2'$, there is a manifold of Σ, Δ, Γ ($K = 0, 2, 4, \ldots$), etc., levels, and for even v$_2'$, there are Π, Φ, H ($K = 1, 3, 5, \ldots$), etc. levels. Since we observe that jet-cooling populates primarily the $K''_a = 0$ and 1 stacks of rotational levels, only transitions to the upper state $K = 0$ (Σ), $K = 1$ (Π), and $K = 2$ (Δ) levels are expected. This means that only a single Π band is expected for even v$_2'$ but transitions to odd v$_2'$ should consist of closely spaced Σ and Δ subbands as is found for (0,15,0) of ^{11}BD$_2$ and shown in Fig. 5. According to Pople and
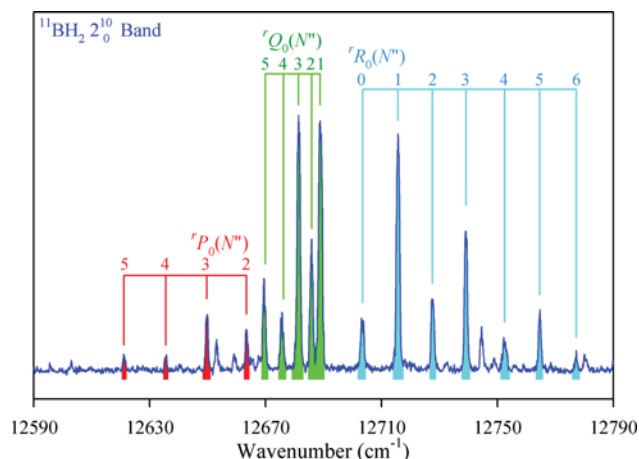

FIG. 4. The medium-resolution sync-scan LIF spectrum of the 2_0^{10} Π band of ^{11}BH$_2$. The vertical leaders identify the rotational branches and assignments.
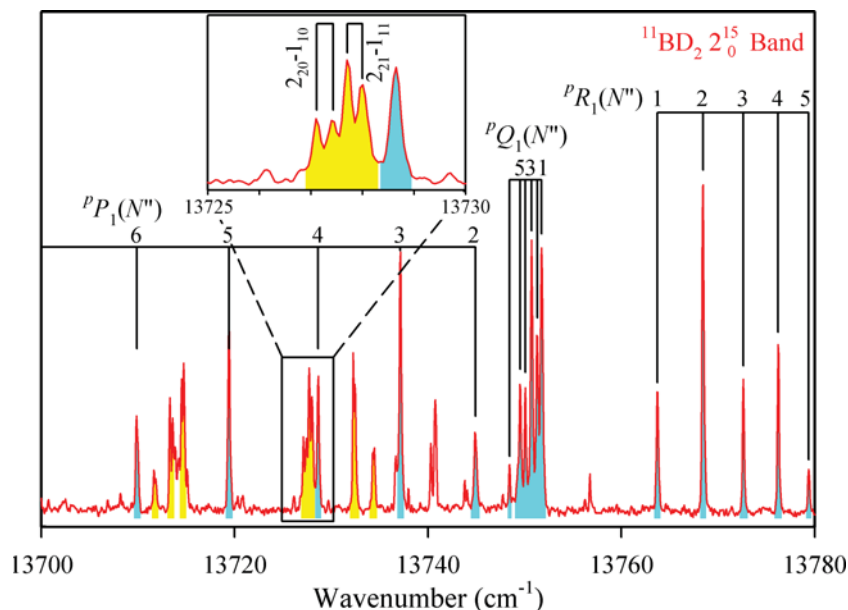
FIG. 5. Medium resolution LIF spectra of the 2_0^{15} band of $^{11}BD_2$. The leaders identify the branches of the Σ band (darker shading, shaded blue online). Some of the rotational lines of the nearby Δ band at lower energies are also identified (lighter shading, shaded yellow online). The inset shows the four spin- and asymmetry-split components of the $^rR_1(1)$ transition of the Δ band.

Longuet-Higgins,[32] such upper state vibrational levels with $v_2 > K$ can be represented by

$$G(v_2, K) = \omega_2(v_2 + 1) + x_{22}(v_2 + 1)^2 - GK^2, \quad (1)$$

where G is a positive quantity depending on the potential constants. This equation implies that the Δ subband should be below the Σ, as is observed. The major difference between the Σ and Δ bands is that the latter show characteristic asymmetry splittings. For example, the $^rR_1(1)$ transition must consist of two lines, $2_{2,1} \leftarrow 1_{1,0}$ and $2_{2,0} \leftarrow 1_{1,1}$ with a consistent splitting of ~ 0.6 cm^{-1} (~ 1.2 cm^{-1} for $^{11}BH_2$). As is shown in the inset to Fig. 5, this line actually consists of four components, as the asymmetry components are further spin-split.

In their original work, Herzberg and Johns[15] only found spin doublings in the $(0,9,0)$ $\Delta - \Pi$ band at 11 700 cm^{-1}, with an interval of about 0.3 cm^{-1}. In our work, we were able to identify spin splittings in several of the bands terminating on Π or Δ states. It is clear from our calculations and those of others[18,19] that the spin multiplets in the lowest vibrational level of the ground state are regular with the energy of the $J = N + 1/2(F_1)$ component higher than that of $J = N - 1/2(F_2)$ for a given $N_{Ka,Kc}$ and there is no appreciable spin splitting for the $K_a'' = 0$ levels. In the excited state, the Σ $(K = 0)$ levels are also not spin-split but the higher K $(\Pi, \Delta, \dots)$ levels often have appreciable spin splittings, which may be regular or inverted depending on the identity of the vibrational state and whether or not it is perturbed. We have assigned the J quantum numbers in our spectra based on the relative intensities at the beginning of the branch, with the usual expectation that $\Delta J = \Delta N$ transitions should be strongest, and that transitions originating in the F_1 levels should be more intense than those from F_2 due to the greater $2J + 1$ degeneracy of the former. For example, the $(0,14,0)\Pi$ band shows spin splittings in all the branches. The $^rR_0(0)$ transition has two lines at 16 383.80 cm^{-1} (intensity = 1.7) and 16 385.09 cm^{-1} (intensity = 1.0) with a splitting of 1.29 cm^{-1}. The higher intensity line is assigned as $J = 1.5 \leftarrow J = 0.5$ ($\Delta J = \Delta N$) and the weaker as $J = 0.5 \leftarrow J = 0.5$ so that the upper state

level is inverted with the energy of $J = 0.5 > J = 1.5$. The next $^rR_0(1)$ line has a spin splitting of 0.73 cm^{-1} with the lower wavenumber line stronger than the higher wavenumber feature. The lower state levels have $J = 1.5$ ($2J + 1 = 4$) and $J = 0.5$ ($2J + 1 = 2$) so the transitions are assigned as $J = 2.5 \leftarrow J = 1.5$ (lower) and $J = 1.5 \leftarrow J = 0.5$ (upper), again inverted. The fact that the $^rP_0(2)$ and $^rP_0(3)$ transitions have the same measured spin-splittings as those of $^rR_0(0)$ and $^rR_0(1)$ proves that the lower state $K = 0$ levels are not spin-split. In this fashion, J values were assigned to all the spin-split transitions in our LIF spectra.

In the expected region of the $(0,14,0)$ Π band of $^{11}BH_2$, we observed two Π bands, whose $^rR_0(0)$ transitions (see Table I) are separated by 91.5 cm^{-1} and have opposite spin-splittings in the upper state such that the lower energy band has inverted spin levels, whereas the higher is regular. Initially, it proved difficult to make upper state vibronic assignments of these two bands but once the *ab initio* calculations of the spin-rovibronic levels were available (*vide infra*), the cause of the anomaly was clear. The calculations show that there is a strong, almost 50:50 mixing of the excited state $(0,14,0)$ $K = 1$ rotational levels with the higher $(0,13,0)$ $K_a = 1$ levels of the ground state so that transitions to the latter gain intensity and can be observed experimentally. The calculated upper state energies agree with the measured transition frequencies (see Table I) and the observed and calculated $^rR_0(0)$ spin splittings agree in sign and magnitude ($\tilde{A}(0,14,0)$: obs = -1.3 cm^{-1}, calc = -0.99 cm^{-1}; $\tilde{X}(0,13,0)$: obs = $+1.1$ cm^{-1}, calc = $+1.03$ cm^{-1}). There can be little doubt that the assignments are correct. In a similar fashion, we were able to assign a pair of $^{11}BD_2$ bands at 14 443 and 14 509 cm^{-1} as transitions to $\tilde{A}(0,16,0)$ and $\tilde{X}(0,16,0)$, respectively.

In summary, we have assigned 67 bands of the four isotopologues of BH_2. In addition, there are a variety of weak band fragments, groups of lines, and even single lines scattered throughout the spectra which have no detailed assignments. In order to make comparisons with our theoretical predictions, we report in Tables I and II the specific

TABLE I. A comparison of the experimentally measured transition frequencies (in cm^{-1}) of the assigned LIF bands of $^{11}BH_2$ and $^{10}BH_2$ and their theoretically predicted values.

Band	$^{11}BH_2$		$^{10}BH_2$	
	Expt.[a]	Theory[b]	Expt.	Theory[c]
$(0,9,0)\Sigma$	11 718.72*	11 717.9	11 779.72*	11 775.1
$(0,9,0)\Delta$	11 717.18*	11 714.2	...	11 776.3
$(0,10,0)\Pi$	12 703.48	12 701.7	...	12 763.6
$(0,11,0)\Sigma$	13 591.94	13 591.5	13 660.08	13 658.7
$(0,11,0)\Delta$	13 569.62	13 568.8	...	13 632.3
$(0,12,0)\Pi$	14 570.80	14 569.9	14 641.36	14 638.7
$(1,10,0)\Pi$	15 217.97[d]	15 218.5	...	15 292.9
$(0,13,0)\Sigma$	15 457.34	15 457.0	15 530.87	15 533.0
$(0,13,0)\Delta$	15 414.28/15.19	15 416.3	...	15 495.1
$(1,11,0)\Sigma$	16 102.77	16 103.8	...	16 176.3
$(0,14,0)\Pi$	16 383.80/85.09	16 386.9	...	16 480.3
X$(0,13,0)$[e]	164 75.43/76.53	16 475.7	16 571.69[d]	16 571.0
$(1,12,0)\Pi$	17 065.61	17 070.7	...	17 149.7
$(0,15,0)\Sigma$	17 314.49	17 314.6	17 398.75	17 398.7
$(0,15,0)\Delta$	17 337.03/37.79	17 335.7	17 426.24/27.09	17 424.9
$(1,13,0)\Sigma$	17 949.23	17 951.0	...	18 032.8
$(0,16,0)\Pi$	18 294.74/95.06	18 292.5	18 385.00	18 385.5
$(1,14,0)\Pi$	18 927.16/27.56	18 926.1	...	19 014.6
$(0,17,0)\Sigma$	19 163.63	19 163.9	19 255.27	19 255.5
$(0,17,0)\Delta$	19 163.03	19 163.2	19 256.12	19 256.0
$(0,18,0)\Pi$	20 134.76	20 134.3	20 231.69	20 231.0
$(0,19,0)\Sigma$	21 003.69	21 004.9	...	21 103.2
$(0,19,0)\Delta$	20 997.10	20 999.6	...	21 099.2

[a]For Σ bands this is $^PP_1(1)$, for Π bands $^rR_0(0)$, and for Δ bands $= ^rR_1(1)$. Both values are reported for spin-split transitions. All measurements ±0.1 cm^{-1}. Experimental values with * from Ref. 15.
[b]For Σ and Δ states, 48.5 cm^{-1} (average of the two spin components of the ground state 1_{10} level) has been subtracted.
[c]For Σ and Δ states, 49.1 cm^{-1} (average of the two spin components of the ground state 1_{10} level) has been subtracted.
[d]Tentative assignment, overlapped or otherwise complicated.
[e]Transition to ground state level.

rovibronic transition in each band that is from the lowest accessible ground state rotational level to the lowest energy accessible upper state rotational level. For Σ bands, this is $\tilde{A}(0_{00}) - \tilde{X}(1_{10}) = ^PP_1(1)$, for Π bands $= \tilde{A}(1_{10}) - \tilde{X}(0_{00}) = ^rR_0(0)$, and Δ bands $= \tilde{A}(2_{20}) - \tilde{X}(1_{10}) = ^rR_1(1)$. If the line is spin-split, then the frequencies of both spin-components are reported. We have elected not to fit the rotational lines of each band to any particular energy level formula as preliminary studies showed that most of the bands were perturbed in some fashion, making the constants unreliable. Instead, the detailed line assignments for all the bands we have analyzed have been given in the supplementary material.[33]

C. High resolution LIF spectra

In previous work, the ground state rotational constants of $^{11}BD_2$ were necessarily very imprecise,[15] which hindered the determination of an accurate molecular structure. In an effort to rectify this deficiency, we recorded high resolution spectra of the $\Pi - \Sigma$ ($K = 1 - K_a = 0$) and $\Pi - \Delta$ ($K = 1 - K_a = 2$) subbands of the 2_0^{20} band of $^{11}BD_2$. Portions of these spectra are shown in Fig. 6 along with the assignments. The $K' = 1 - K_a'' = 0$ subband is quite strong, and the P-, Q-, and R-branches are readily identified, including the very small spin-splittings at low N. In contrast, the $K' = 1 - K_a'' = 2$ subband is very weak, primarily due to the efficient cooling which

depopulates the $K_a'' = 2$ levels, but the branches, which include asymmetry and spin-splittings, were reliably identified using GSCDs. We then fitted the GSCDs to obtain a set of v$''$ = 0 rotational constants for $^{11}BD_2$ which are given along with the previous $^{11}BH_2$ constants[15] in Table III. The individual line measurements and assignments are given in Table IV.

IV. THEORETICAL CALCULATIONS

A. Calculation of the potential energy surfaces

The Potential Energy Surfaces (PESs) for the bent ground $\tilde{X}^2A_1$ and the linear $\tilde{A}^2B_1$ first excited states of BH_2 were constructed from the fit of a large number of single point energy calculations. The geometries of the single point calculations were carefully chosen in order to properly map both PESs for energies up to 22 000 cm^{-1} above the minimum of the $\tilde{X}^2A_1$ state. In summary, 777 points were calculated for the $\tilde{X}^2A_1$ state and 461 points for the $\tilde{A}^2B_1$ state. The geometries were in the ranges $1.6 \leq r_{BH1} \leq 3.7$ bohrs, with $r_{BH2} \geq r_{BH1}$, for the stretching coordinates (all states) and $60 \leq \theta_{HBH} \leq 180$ ($\tilde{X}^2A_1$) or $90 \leq \theta_{HBH} \leq 180$ ($\tilde{A}^2B_1$). The total energy E at each geometry was obtained in a stepwise manner, such that

$$E = E_{V5Z} + \Delta E_{CC} + \Delta E_{CBS} + \Delta E_{FCI} + \Delta E_{BO}, \quad (2)$$

TABLE II. A comparison of the experimentally measured transition frequencies (in cm^{-1}) of the assigned LIF bands of $^{11}BD_2$ and $^{10}BD_2$ and their theoretically predicted values.

| Band | $^{11}BD_2$ | | $^{10}BD_2$ | |
	Expt.[a]	Theory[b]	Expt.[a]	Theory[c]
$(0,14,0)\Pi$	13 073.69/74.00	13 069.3	...	13 172.4
$(1,12,0)\Pi$	13 529.58/29.87	13 526.4	...	13 631.7
$(0,15,0)\Sigma$	13 744.90	13 741.2	13 851.77	13 847.8
$(0,15,0)\Delta$	13 727.11/27.43	13 725.1	...	13 840.4
$(1,13,0)\Sigma$	14 197.11	14 194.0	14 299.96	14 298.3
$(1,13,0)\Delta$	14 180.84/81.05	14 180.2	...	14 287.6
$(0,16,0)\Pi$	14 443.14/44.30	14 441.7	14 564.97/65.83	14 562.1
$X(0,16,0)$[d]	14 508.68/09.81	14 506.6	...	14 653.9
$(0,17,0)\Sigma$	15 130.00	15 126.3	15 245.95	15 242.4
$(0,17,0)\Delta$	15 144.21/44.98	15 140.9	...	15 266.1
$(1,15,0)\Sigma$	15 583.88	15 581.0	...	15 695.9
$(0,18,0)\Pi$	15 849.23	15 846.2	15 971.43	15 967.4
$(1,16,0)\Pi$	16 307.75/08.25	16 305.7	...	16 433.3
$(0,19,0)\Sigma$	16 507.57	16 504.1	16 632.32[e]	16 629.0
$(0,19,0)\Delta$	16 505.66	16 502.3	16 632.32[e]	16 628.9
$(1,17,0)\Sigma$	16 962.52	16 959.9	...	17 084.6
$(1,17,0)\Delta$	16 959.17	16 955.8	...	17 085.6
$(0,20,0)\Pi$	17 220.61	17 216.9	17 351.25	17 347.3
$(1,18,0)\Pi$	17 662.91/63.35	17 663.1	...	17 800.9
$(0,21,0)\Sigma$	17 877.95[e]	17 874.5	18 011.20	18 007.6
$(0,21,0)\Delta$	17 871.32	17 868.9	...	18 004.7
$(1,19,0)\Sigma$	18 332.75	18 330.8	...	18 464.8
$(1,19,0)\Delta$	18 330.84	18 328.6	...	18 467.6
$(0,22,0)\Pi$	18 585.52/85.87	18 582.5	18 723.86/24.16	18 720.6
$(1,20,0)\Pi$	19 057.50	19 040.9	...	19 178.8
$(0,23,0)\Sigma$	19 241.41	19 237.9	...	19 378.6

[a]For Σ bands this is $^PP_1(1)$, for Π bands $^rR_0(0)$, and for Δ bands $= {}^rR_1(1)$. Both values are reported for spin-split transitions. All measurements ±0.1 cm^{-1}.
[b]For Σ and Δ states, 27.3 cm^{-1} (average of the two spin components of the ground state 1_{10} level) has been subtracted.
[c]For Σ and Δ states, 27.8 cm^{-1} (average of the two spin components of the ground state 1_{10} level) has been subtracted.
[d]Transition to ground state level.
[e]Tentative assignment, overlapped or otherwise complicated.

where E_{V5Z} is the energy calculated at the coupled cluster singles and doubles with perturbative triples [CCSD(T)]level of theory[35] with the aug-cc-pV5Z basis,[34] ΔE_{CC} is a correction for the correlation effects of core electrons, ΔE_{CBS} is an estimate of the complete basis set limit within the frozen core approximation, ΔE_{FCI} is an estimate of electron correlation

beyond CCSD(T), and ΔE_{BO} takes into account diagonal Born-Oppenheimer corrections.

The ΔE_{CC} correction was determined by taking the difference between energies at the CCSD(T) level, calculated either with all electrons correlated and the aug-cc-pwCV5Z basis[36] or with valence electrons only and the aug-cc-pV5Z
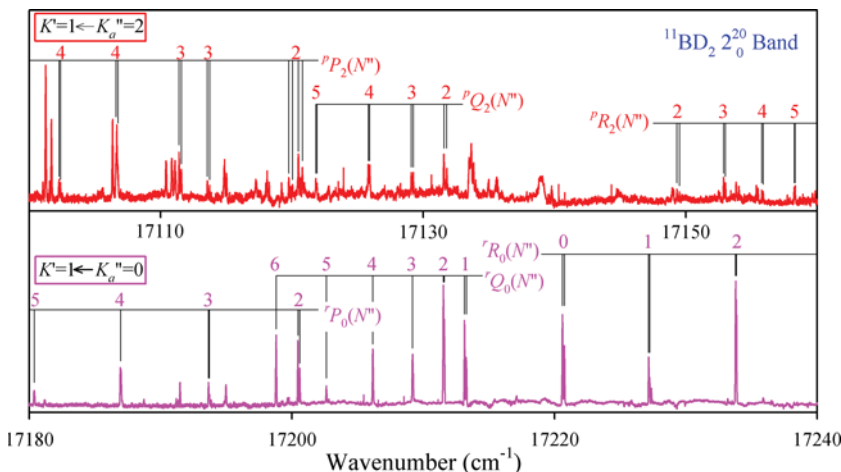

FIG. 6. High resolution LIF spectra of the two Π subbands of the 2_0^{20} transition of $^{11}BD_2$. The upper trace shows the $K_a = 1 - 2$ subband which exhibits resolved spin- and asymmetry-splittings in the various branches. The lower trace is the much stronger $K_a = 1 - 0$ subband which shows partially resolved spin-splittings at low N.

TABLE III. The effective ground state rotational constants of BH_2 and BD_2. All values reported in this table are in cm^{-1}.

Rotational constant	$^{11}BH_2$	$^{11}BD_2$
A_0	41.649(8)[a]	23.321(1)
B_0	7.241(1)	3.627(2)
C_0	6.001(2)	3.094(2)

[a] BH_2 values from Ref. 15, BD_2 from this work. The corresponding theoretical rotational constants are: $A_0 = 42.0541$ cm^{-1}, $B_0 = 7.2330$ cm^{-1}, $C_0 = 6.0175$ cm^{-1} for $^{11}BH_2$, and $A_0 = 23.7301$ cm^{-1}, $B_0 = 3.6287$ cm^{-1}, $C_0 = 3.0931$ cm^{-1}, for $^{11}BD_2$. These in turn have been evaluated from the theoretical equilibrium geometry (see Table VII) by applying second order perturbation theory to the analytical PESs.

basis. The ΔE_{CBS} correction was obtained from the energies calculated at the CCSD(T) level with the aug-cc-pVQZ and aug-cc-pV5Z basis sets,[34] by performing an extrapolation towards the complete basis set limit using the procedure outlined by of the Schwenke.[37]

For the ΔE_{FCI} term, a full CI computation[38] was performed with the cc-pVTZ basis, and the difference between full CI and CCSD(T) energies, with the same basis, was taken. For computational reasons, only valence electrons were correlated and only geometries which can be handled in C_{2v} symmetry by the quantum chemistry package were considered. These include all linear geometries and a subset of bent geometries, those with both r_{BH} bond lengths kept fixed at 2.2 bohrs. The ΔE_{FCI} correction at any geometry was then approximated as

$$\Delta E_{FCI}(r_1, r_2, \theta) = \Delta E_{FCI}(r_1, r_2, 180°) + [\Delta E_{FCI}(2.2, 2.2, \theta) \\ - \Delta E_{FCI}(2.2, 2.2, 180°)], \quad (3)$$

where r_1, r_2 correspond to the r_{BH1} and r_{BH2} bond lengths and θ is the θ_{HBH} angle.

The last ΔE_{BO} term accounts for isotope-dependent diagonal Born-Oppenheimer corrections[39] to the adiabatic surfaces. It was evaluated by calculating the geometry dependence, at the CASSCF/aug-cc-pwCV5Z level, of the $\hat{L}_x^2, \hat{L}_y^2, \hat{L}_z^2$, and $\hat{L}_x\hat{L}_z$ angular momentum operator matrix elements, as exploited in Eq. (1b) of Ref. 40. Their values are usually taken as zero for the $\hat{L}_x^2, \hat{L}_y^2$, and $\hat{L}_x\hat{L}_z$ operators and one for $\hat{L}_z^2$ operator, for all geometries. The influence of the inclusion of the geometry dependence of these operators has been discussed in detail in Ref. 41. The ΔE_{BO} term depends on the masses of the atoms and it has been computed from the following equation:[40,42]

$$\Delta E_{BO}^k(r_1, r_2, \theta) = \frac{1}{8 \cos^2(\theta/2)} \left(\frac{1}{\mu_1 r_1^2} + \frac{1}{\mu_2 r_2^2} + \frac{2}{m r_1 r_2} \right) \\ \times (\langle k|\hat{L}_z^2|k \rangle - 1) \\ + \frac{1}{8 \sin^2(\theta/2)} \left(\frac{1}{\mu_1 r_1^2} + \frac{1}{\mu_2 r_2^2} - \frac{2}{m r_1 r_2} \right) \\ \times \langle k|\hat{L}_x^2|k \rangle \\ + \frac{1}{8} \left(\frac{1}{\mu_1 r_1^2} + \frac{1}{\mu_2 r_2^2} + \frac{2 \cos \theta}{m r_1 r_2} \right) \langle k|\hat{L}_y^2|k \rangle \\ - \frac{1}{4 \sin \theta} \left(\frac{1}{\mu_1 r_1^2} - \frac{1}{\mu_2 r_2^2} \right) \\ \times \langle k|\hat{L}_x\hat{L}_z + \hat{L}_z\hat{L}_x|k \rangle, \quad k = \tilde{X}^2 A_1, \tilde{A}^2 B_1, \quad (4)$$

where r_1, r_2 correspond to the r_{BH1} and r_{BH2} bond lengths, θ is the θ_{HBH} angle, m is the mass of the central B atom, and μ_1 and μ_2 are the reduced masses between the central B atom and the peripheral H1 and H2 atoms (see Ref. 40 for further details).

All the CCSD(T) calculations needed to set up Eq. (2) were performed with the CFOUR suite of quantum chemistry programs.[43] Full CI energies and angular momentum matrix elements were obtained with the Molpro 2010 code.[44]

The discrete energies of the two states, as defined by Eq. (2), were fitted using the SURFIT program,[45] using symmetry restricted polynomial functions with the general form

$$V^\eta(r_1, r_2, \theta) = \sum_{ijk} c_{ijk}^\eta (q_1 - q_1^{ref,\eta})^i (q_2 - q_2^{ref,\eta})^j (q_3 - q_3^{ref,\eta})^k,$$
$$(5)$$

where η refers to a specific electronic state and isotopologue, $q_1 = (r_1 + r_2)/\sqrt{2}$ (symmetric stretch), $q_2 = (r_1 - r_2)/\sqrt{2}$ (antisymmetric stretch), and $q_3 = \theta_{HBH}$; $q_1^{ref,\eta}$, $q_2^{ref,\eta}$, and $q_3^{ref,\eta}$ define the reference geometry of the η-th state. Symmetry restrictions constrain j to be even for both states and k to be even for the $\tilde{A}^2 B_1$ state. The two PESs of four different isotopologues ($^{11}BH_2$, $^{10}BH_2$, $^{11}BD_2$, $^{10}DB_2$) have been obtained in this way and the corresponding fitting coefficients c_{ijk}^η are reported with and without the mass-dependent corrections as supplementary material.[33] The root mean square deviations (RMSDs) of the fittings were 4.1 cm^{-1} for the lower ($\tilde{X}^2 A_1$, ground state) surface and 0.6 cm^{-1} for the upper ($\tilde{A}^2 B_1$ excited state) surface. The degeneracy of the two surfaces at linearity was imposed by simply including 52 linear geometries ($1.7 \leq r_{BH1} \leq 2.8$ bohrs, $r_{BH2} \geq r_{BH1}$) in the fitting of the ground state coefficients. This procedure was much simpler than that adopted previously for HBF,[11] and it was able to recover surfaces which are nearly degenerative for linear geometries, with differences of the same order of magnitude of the RMSDs of the fittings. These tiny differences proved to be irrelevant in the subsequent variational calculation of the rovibronic energy levels.

The Molpro code was also used to calculate the phenomenological spin-orbit splitting of the electronic Π ($\tilde{X}^2 A_1$, $\tilde{A}^2 B_1$) state. At the computed equilibrium geometry of the $\tilde{A}^2 B_1$ state, using the CASSCF level of theory and the aug-cc-pV5Z basis, the splitting was 7.72 cm^{-1}, which is in a very good agreement with the empirical value of 7.93 cm^{-1} found by Kolbuszewski *et al.*[19] This was taken as a geometry independent parameter and used in all subsequent variational calculations.

B. Calculation of the rovibronic energy levels

The *ab initio* surfaces were used for the variational calculation of the rovibronic energy levels. Preliminary analyses were performed using the RVIB3 code developed by Carter and co-workers.[46] However, in the course of these tests, a paper by Mitrushchenkov was published,[47] pointing out some numerical difficulties in the RVIB3 code and its underlying theory in the handling of cases with very large Renner-Teller coupling, such as linear-bent systems. These difficulties become evident only in the calculation of levels with $K_a > 0$ (Π, Δ, etc., states). We then resorted to using a

TABLE IV. The individual transition measurements and assignments from the high-resolution LIF spectrum of the 2_0^{20} band of $^{11}BD_2$.

	Branch	N', K_a', K_c', J'	N'', K_a'', K_c'', J''	Line position
$K' = 1 \leftarrow K_a'' = 0$	$^r R_0(0)$	1, 1, 0, 1.5	0, 0, 0, 0.5	17 220.597
	$^r R_0(0)$	1, 1, 0, 0.5	0, 0, 0, 0.5	17 220.743
	$^r R_0(1)$	2, 1, 1, 2.5	1, 0, 1, 1.5	17 227.164?
	$^r R_0(1)$	2, 1, 1, 1.5	1, 0, 1, 0.5	17 227.229?
	$^r R_0(2)$	3, 1, 2, 3.5	2, 0, 2, 2.5	17 233.783
	$^r R_0(2)$	3, 1, 2, 2.5	2, 0, 2, 1.5	17 233.836
	$^r R_0(3)$	4, 1, 3[a]	3, 0, 3	17 240.458
	$^r R_0(4)$	5, 1, 4	4, 0, 4	17 247.255
	$^r Q_0(1)$	1, 1, 1, 1.5	1, 0, 1, 1.5	17 213.138
	$^r Q_0(1)$	1, 1, 1, 0.5	1, 0, 1, 0.5	17 213.276
	$^r Q_0(2)$	2, 1, 2, 2.5	2, 0, 2, 2.5	17 211.528
	$^r Q_0(2)$	2, 1, 2, 1.5	2, 0, 2, 1.5	17 211.591
	$^r Q_0(3)$	3, 1, 3, 3.5	3, 0, 3, 3.5	17 209.168
	$^r Q_0(3)$	3, 1, 3, 2.5	3, 0, 3, 2.5	17 209.186
	$^r Q_0(4)$	4, 1, 4	4, 0, 4	17 206.155
	$^r Q_0(5)$	5, 1, 5	5, 0, 5	17 206.616
	$^r Q_0(6)$	6, 1, 6	6, 0, 6	17 198.787
	$^r P_0(2)$	1, 1, 0, 1.5	2, 0, 2, 2.5	17 200.447
	$^r P_0(2)$	1, 1, 0, 0.5	2, 0, 2, 1.5	17 200.591
	$^r P_0(3)$	2, 1, 1, 2.5	3, 0, 3, 3.5	17 193.693?
	$^r P_0(3)$	2, 1, 1, 1.5	3, 0, 3, 2.5	17 193.704?
	$^r P_0(4)$	3, 1, 2, 3.5	4, 0, 4, 4.5	17 186.926
	$^r P_0(4)$	3, 1, 2, 2.5	4, 0, 4, 3.5	17 186.968
	$^r P_0(5)$	4, 1, 3	5, 0, 5	17 180.367
	$^r P_0(6)$	5, 1, 4	6, 0, 6	17 174.027
$K' = 1 \leftarrow K_a'' = 2$	$^p R_2(2)$	3, 1, 3, 3.5	2, 2, 1, 2.5	17 149.311
	$^p R_2(2)$	3, 1, 3, 2.5	2, 2, 1, 1.5	17 149.503
	$^p R_2(2)$	3, 1, 2, 3.5	2, 2, 0, 2.5	17 153.819
	$^p R_2(2)$	3, 1, 2, 2.5	2, 2, 0, 1.5	17 154.030
	$^p R_2(3)$	4, 1, 4, 4.5	3, 2, 2, 3.5	17 152.871
	$^p R_2(3)$	4, 1, 4, 3.5	3, 2, 2, 2.5	17 153.002
	$^p R_2(3)$	4, 1, 3, 4.5	3, 2, 1, 3.5	17 160.358
	$^p R_2(3)$	4, 1, 3, 3.5	3, 2, 1, 2.5	17 160.507
	$^p R_2(4)$	5, 1, 5, 5.5	4, 2, 3, 4.5	17 155.776
	$^p R_2(4)$	5, 1, 5, 4.5	4, 2, 3, 3.5	17 155.879
	$^p R_2(4)$	5, 1, 4, 5.5	4, 2, 2, 4.5	17 166.898
	$^p R_2(4)$	5, 1, 4, 4.5	4, 2, 2, 3.5	17 167.022
	$^p R_2(5)$	6, 1, 6, 6.5	5, 2, 4, 5.5	17 158.249
	$^p R_2(5)$	6, 1, 6, 5.5	5, 2, 4, 4.5	17 158.313
	$^p Q_2(2)$	2, 1, 2, 2.5	2, 2, 0, 2.5	17 131.563
	$^p Q_2(2)$	2, 1, 2, 1.5	2, 2, 0, 1.5	17 131.784
	$^p Q_2(3)$	3, 1, 2, 3.5	3, 2, 2, 3.5	17 133.652
	$^p Q_2(3)$	3, 1, 2, 2.5	3, 2, 2, 2.5	17 133.820
	$^p Q_2(3)$	3, 1, 3, 3.5	3, 2, 1, 3.5	17 129.092
	$^p Q_2(3)$	3, 1, 3, 2.5	3, 2, 1, 2.5	17 129.226
	$^p Q_2(4)$	4, 1, 4, 4.5	4, 2, 2, 4.5	17 125.809
	$^p Q_2(4)$	4, 1, 4, 3.5	4, 2, 2, 3.5	17 125.914
	$^p Q_2(5)$	5, 1, 5, 5.5	5, 2, 3, 5.5	17 121.818
	$^p Q_2(5)$	5, 1, 5, 4.5	5, 2, 3, 4.5	17 121.895
	$^p Q_2(5)$	5, 1, 4, 5.5	5, 2, 4, 5.5	17 133.478
	$^p Q_2(5)$	5, 1, 4, 4.5	5, 2, 4, 4.5	OL[b]
	$^p P_2(2)$	1, 1, 0, 1.5	2, 2, 0, 2.5	17 120.480
	$^p P_2(2)$	1, 1, 0, 0.5	2, 2, 0, 1.5	17 120.785
	$^p P_2(2)$	1, 1, 1, 1.5	2, 2, 1, 2.5	17 119.752
	$^p P_2(2)$	1, 1, 1, 0.5	2, 2, 1, 1.5	17 120.035
	$^p P_2(3)$	2, 1, 1, 2.5	3, 2, 1, 3.5	17 113.554
	$^p P_2(3)$	2, 1, 1, 1.5	3, 2, 1, 2.5	17 113.732
	$^p P_2(3)$	2, 1, 2, 2.5	3, 2, 2, 3.5	17 111.400
	$^p P_2(3)$	2, 1, 2, 1.5	3, 2, 2, 2.5	17 111.572

TABLE IV. (*Continued.*)

Branch	N', K_a', K_c', J'	N'', K_a'', K_c'', J''	Line position
$^PP_2(4)$	3, 1, 2, 3.5	4, 2, 2, 4.5	17 106.592
$^PP_2(4)$	3, 1, 2, 2.5	4, 2, 2, 3.5	17 106.740
$^PP_2(4)$	3, 1, 3, 3.5	4, 2, 3, 4.5	17 102.247
$^PP_2(4)$	3, 1, 3, 2.5	4, 2, 3, 3.5	17 102.364
$^PP_2(5)$	4, 1, 3, 4.5	5, 2, 3, 5.5	17 099.543
$^PP_2(5)$	4, 1, 3, 3.5	5, 2, 3, 4.5	17 099.649
$^PP_2(5)$	4, 1, 4, 4.5	5, 2, 4, 5.5	17 092.374(OL)
$^PP_2(5)$	4, 1, 4, 3.5	5, 2, 4, 4.5	17 092.461(OL)

[a]The J quantum number is omitted from transitions that did not exhibit resolved splittings. Transitions with a question mark are perturbed or otherwise irregular.
[b]OL = overlapped.

previous version of the code, based on a different definition of the basis set for the bending motion,[40] which has proved to work correctly for linear-bent systems.[18,41]

The variational basis set of the two electronic states was built from 20 harmonic oscillators for the stretches and 104 Legendre polynomials for the bend, contracted to 25 two-dimensional stretching functions and 61 two dimensional bending functions.

Spin-rovibronic calculations for $J = 1/2, 3/2, 5/2$, and $7/2$ were performed, thus enabling the prediction of the energies for all rovibrational levels with $K_a \leq 3$ ($\Sigma, \Pi, \Delta, \Phi$ levels). The vibrational quantum numbers were assigned by inspection of the variational coefficients and, for higher levels, by counting the nodes in plots of the vibrational wavefunctions. All four experimentally relevant isotopologues ($^{11}BH_2$, $^{10}BH_2$, $^{11}BD_2$, $^{10}BD_2$) were studied, for energies up to 22 000 cm^{-1} above the $\tilde{X}^2A_1(000)$ level.

The comparison between the observed and calculated transition frequencies for the various observed bands of BH_2 and BD_2 is presented in Tables I and II. The agreement between the two quantities is excellent, with differences of only a few cm^{-1} in each case. We show in Tables V and VI, the lowest calculated vibrational levels of the ground state and the calculated pure bending levels of the excited state up to 22 000 cm^{-1}, respectively. The relevant results of the present

TABLE V. Calculated low-lying $\tilde{X}^2A_1$ state vibrational energy levels ($N_{Ka,Kc} = 0_{00}$) of the various BH_2 isotopologues (in cm^{-1}).

(v_1,v_2,v_3)	$^{11}BH_2$	$^{11}BD_2$	$^{10}BH_2$	$^{10}BD_2$
(0,1,0)	972.9	733.0	979.1	740.5
(0,2,0)	1910.9	1435.6	1923.4	1450.1
(1,0,0)	2508.1	1818.4	2511.6	1823.6
(0,0,1)	2658.4	2017.3	2674.8	2039.5
(0,3,0)	2857.4	2114.0	2877.5	2135.9
(1,1,0)	3482.1	2552.8	3492.0	2565.9
(0,1,1)	3630.9	2750.9	3653.5	2780.6
(0,4,0)	3866.2	2795.7	3894.7	2826.5
(1,2,0)	4421.9	3256.3	4438.5	3276.6
(0,2,1)	4566.8	3455.8	4595.5	3492.4
(0,5,0)	4951.1	3514.2	4988.0	3555.1
(2,0,0)	4964.6	3612.4	4971.7	3622.8
(1,0,1)	5078.4	3790.2	5097.9	3817.4
(0,0,2)	5270.1	4003.7	5301.4	4046.9

ab initio computations compared to previous studies[18,19] are summarized in Table VII.

V. DISCUSSION

A. Molecular structure

The determination of the ground state rotational constants of two different isotopomers of $^{11}BH_2$ allows a precise evaluation of the effective zero-point molecular structure. Planar moments ($P_{A,B,\text{ or }C}$), rather than the raw rotational constants or moments of inertia, were used for the least squares analysis to minimize correlations between the geometric parameters. Since the out-of-plane planar moment P_C must by definition be zero, the data set included only P_A and P_B of $^{11}BH_2$ and $^{11}BD_2$. Allowance was made for a slight decrease (0.003 Å) in the B–H bond length upon deuteration. The resulting structure is

$$r_0(BH) = 1.197(2) \text{ Å}, \qquad \theta_0 = 129.6(2)°,$$

where the numbers in parentheses are one standard error. The agreement between the experimental and *ab initio* values of $r_0(BH) = 1.195$ Å and $\theta_0 = 129.9°$ is excellent. (The *ab initio* values have been obtained by applying the same analysis to the theoretical rotational constants as reported in the footnote to Table III.) The BH bond length is 0.017 Å shorter than that of the HBF free radical[48] and is ~0.035 Å shorter than the equilibrium ground state bond length (1.2322 Å) of the BH radical.[49] The short BH bond length is entirely consistent with a BH_2 symmetric stretching frequency of 2508 cm^{-1} (Table VII) which is substantially larger than the $\omega_1^0 = 2433$ and $\omega_e = 2366.7$ cm^{-1} BH stretching frequencies of HBF and BH, respectively. The BH_2 bond length is almost identical to the $r_0 = 1.190$ Å bond length of gas phase BH_3.[50]

B. Comparison between theory and experiment

In contrast to previous theoretical studies,[18,19] no attempts were made to improve our *ab initio* surfaces empirically. Nevertheless, the accuracy of the calculated vibronic levels is similar to that routinely obtainable in pure vibrational spectroscopy applications, i.e., better than 5 cm^{-1}. To our knowledge, such accuracy has never before been reached in computational spectroscopy studies of Renner-Teller molecules.

TABLE VI. Calculated $\tilde{A}^2B_1$ state vibronic ($N = K_a$) bending levels, relative to the lowest rovibrational level of the electronic ground state, of the BH_2 isotopologues (in cm^{-1}). For Π, Δ, and Φ states, the average of K_c and spin components is reported.

(v_1,v_2,v_3)	$^{11}BH_2$	$^{11}BD_2$	$^{10}BH_2$	$^{10}BD_2$
$(0, 1, 0)\Sigma$	4 191.6	3 834.7	4 203.2	3 850.0
$(0, 2, 0)\Pi$	5 076.3	4 489.0	5 096.4	4 517.7
$(0, 3, 0)\Delta$	5 850.1	5 019.3	5 879.3	5 064.9
$(0, 3, 0)\Sigma$	6 097.6	5 283.1	6 122.5	5 315.3
$(0, 4, 0)\Phi$	6 602.6	5 826.8	6 641.6	5 875.9
$(0, 4, 0)\Pi$	7 061.6	5 985.1	7 098.5	6 027.7
$(0, 5, 0)\Delta$	7 924.2	6 623.9	7 964.6	6 675.1
$(0, 5, 0)\Sigma$	7 995.4	6 720.4	8 032.3	6 768.0
$(0, 6, 0)\Phi$	8 761.3	7 179.9	8 808.0	7 250.1
$(0, 6, 0)\Pi$	8 917.6	7 373.0	8 961.4	7 437.2
$(0, 7, 0)\Delta$	9 789.5	8 140.1	9 839.6	8 212.9
$(0, 7, 0)\Sigma$	9 884.9	8 147.7	9 933.0	8 209.2
$(0, 8, 0)\Phi$	10 664.1	8 781.4	10 718.2	8 857.1
$(0, 8, 0)\Pi$	10 854.9	8 849.4	10 913.0	8 918.9
$(0, 9, 0)\Delta$	11 762.7	9 514.7	11 825.4	9 593.8
$(0, 9, 0)\Sigma$	11 766.4	9 565.7	11 824.8	9 640.0
$(0, 10, 0)\Phi$	12 654.4	10 151.8	12 720.6	10 238.9
$(0, 10, 0)\Pi$	12 701.7	10 265.9	12 763.6	10 345.4
$(0, 11, 0)\Delta$	13 617.2	10 900.6	13 681.4	10 995.8
$(0, 11, 0)\Sigma$	13 639.9	10 974.8	13 707.8	11 060.9
$(0, 12, 0)\Phi$	14 494.8	11 659.4	14 570.3	11 761.0
$(0, 12, 0)\Pi$	14 569.9	11 676.1	14 638.7	11 768.8
$(0, 13, 0)\Delta$	15 464.7	12 358.5	15 544.2	12 458.7
$(0, 13, 0)\Sigma$	15 505.4	12 375.6	15 582.1	12 472.6
$(0, 14, 0)\Phi$	16 308.3	13 027.9	16 397.8	13 130.5
$(0, 14, 0)\Pi$	16 386.9	13 069.3	16 480.3	13 172.4
$(0, 15, 0)\Delta$	17 384.1	13 752.4	17 474.0	13 868.2
$(0, 15, 0)\Sigma$	17 363.0	13 768.5	17 447.8	13 875.6
$(0, 16, 0)\Phi$	18 292.3	14 390.2	18 402.6	14 512.6
$(0, 16, 0)\Pi$	18 292.5	14 441.7	18 385.5	14 562.1
$(0, 17, 0)\Delta$	19 211.6	15 168.2	19 305.1	15 293.9
$(0, 17, 0)\Sigma$	19 212.4	15 153.6	19 304.6	15 270.2
$(0, 18, 0)\Phi$	20 114.0	15 843.7	20 214.2	15 970.6
$(0, 18, 0)\Pi$	20 134.3	15 846.2	20 231.0	15 967.4
$(0, 19, 0)\Delta$	21 048.0	16 529.6	21 148.3	16 656.7
$(0, 19, 0)\Sigma$	21 053.3	16 531.4	21 152.3	16 656.8
$(0, 20, 0)\Phi$	21 944.1	17 199.7	22 050.4	17 334.5
$(0, 20, 0)\Pi$	21 970.8	17 216.9	22 073.3	17 347.3
$(0, 21, 0)\Delta$		17 896.2		18 032.5
$(0, 21, 0)\Sigma$		17 901.8		18 035.4
$(0, 22, 0)\Phi$		18 556.8		18 699.3
$(0, 22, 0)\Pi$		18 582.4		18 720.6
$(0, 23, 0)\Delta$		19 230.5		19 382.4
$(0, 23, 0)\Sigma$		19 265.1		19 406.4
$(0, 24, 0)\Phi$		19 878.9		20 043.7
$(0, 24, 0)\Pi$		19 950.7		20 099.2
$(0, 25, 0)\Delta$		20 633.7		20 780.0
$(0, 25, 0)\Sigma$		20 621.4		20 761.9

It is shown in Fig. 7 that all the corrections quoted in Eq. (2) are important to achieve such an ambitious result. The figure was constructed using the vibronic levels obtained from preliminary PESs which included only part of the corrections. All the remaining parameters of the Renner-Teller code were kept fixed and the comparison was restricted to the experimentally determined levels of $^{11}BH_2$ reported in Table I.

When the PESs were constructed from points calculated with just the E_{V5Z} energies, a gross overestimation (RMSD = 45.8 cm^{-1}) of the vibronic levels is observed. However, a significant improvement (RMSD = 29.9 cm^{-1}) is obtained by including the contribution of core correlation energy (ΔE_{CC}), while the extrapolation to the complete basis set limit (ΔE_{CBS}) is much less important, since it improves the energies of most levels by only few wavenumbers (RMSD = 28.2 cm^{-1}). The effect of valence electron correlation beyond CCSD(T), ΔE_{FCI}, is comparable to that of core correlation and is mandatory to reach reasonable spectroscopic accuracy (RMSD = 4.5 cm^{-1}). Unfortunately, the calculation of this contribution is particularly time consuming, so only a limited set of geometries in C_{2v} was considered, extrapolating the results to the whole surfaces, using Eq. (3). The inclusion of the mass dependent correction (ΔE_{BO}) is of minor importance but it brings the predicted levels even closer to experiment (RMSD = 2.1 cm^{-1}).

The relevant properties of our PESs are summarized in Table VII, where they are also compared to those reported in Refs. 18 and 19. Both the topological and spectroscopic results are very similar to previous results, with our values slightly closer to those of Kolbuszewski *et al.*[19] However, the overall good accuracy of previous computations is partly due to empirical corrections applied to the *ab initio* PESs, in order to best reproduce the spectroscopic information available at that time. In particular, the barrier to linearity of the $\tilde{X}^2A_1$ state (i.e., the minimum of the $\tilde{A}^2B_1$ state) was lowered by $\sim$100 cm^{-1} in both papers. The practice of making moderate and intelligent adjustments to high level *ab initio* computations is very common, even in the recent literature (see, e.g., Ref. 51 for recent application to the water molecule). This is mainly due to the intrinsic limitations of the computer technology rather than defects of the underlying theories. Usually, these approaches are justified "*ex post facto*" by the good predictive capabilities of the final models. However, care must be taken when the set of data to which the calculations are "tuned" is limited, either in number or in accuracy, since "local" improvements may be achieved at the expense of a global deterioration. In these cases, plain *ab initio* computations, even with limited accuracy, may prove to be more reliable.

In the present work, we aimed to reach the highest possible accuracy using only *ab inito* methods. With current technology, this is possible only combining complementary methods in conjunction with basis sets of different sizes. The overall quality of such a hybrid yet fully *ab initio* approach is clearly depicted by the graph at the bottom of Fig. 7 and by the value of the barrier to linearity reported in Table VII.

Another important aspect of the synergy between theory and experiment in this work was the identification of new, unexpected bands in the LIF spectra of BH_2 and BD_2. In particular, a Π band at $^{11}BH_2$ at 16 475 cm^{-1} and the corresponding band of $^{10}BH_2$ at 16 572 cm^{-1} were assigned as transitions to the ground state $\tilde{X}(0,13,0)$ $K_a = 1$ levels which are heavily mixed with the rotational levels of the (0,14,0) Π vibronic excited state. Similarly, a fragment of a $^{11}BD_2$ band at 14 509 cm^{-1} was identified from the calculations as a transition to the ground state (0,16,0) $K_a = 1$ level which perturbs the

TABLE VII. Summary of relevant theoretical data for $^{11}BH_2$.

| | $\tilde{X}^2A_1$ | | | | | | $\tilde{A}^2B_1$ (Π_u) | | | | |
| | Equilibrium geometry | | Fundamental frequencies/cm^{-1} | | | Barrier to linearity/cm^{-1} | Equilibrium geometry | | Fundamental frequencies/cm^{-1} | | |
	r_{BH}/Å	θ/deg	ν_1	ν_2	ν_3		r_{BH}/Å	T_0/cm^{-1}	ν_1[a]	ν_2[b]	ν_3[c]
Reference 18	1.184	128.68	2518	986	2667	2693[d]	1.167	4216	2597	950	2830
Reference 19	1.1875	129.04	2506.5	972.8	2657.9	2666[e]	1.1698	4203.9	2589.7	950.7	2825.1
This work	1.1844[f]	129.05[f]	2508.1	972.9	2658.4	2655.7[g]	1.1674[f]	4191.6	2592.1	953.0	2829.0

[a]The difference $A(1,1,0)\Sigma - A(0,1,0)\Sigma$ is reported.
[b]The value $1/2[A(0,3,0)\Sigma - A(0,1,0)\Sigma]$ is reported.
[c]The difference $A(0,1,1)\Sigma - A(0,1,0)\Sigma$ is reported.
[d]This value is empirically corrected. The *ab initio* value is 2790 cm^{-1}.
[e]This value is empirically corrected. The *ab initio* value is 2743 cm^{-1}.
[f]Minima of the analytical PESs without mass dependent corrections.
[g]*Ab initio* value obtained as difference between the energy minima of the analytical PESs without mass dependent corrections.

$\tilde{A}(0,16,0)$ Π vibronic state. Such assignments would not have been possible without the very precise calculations reported in the present work.

In their very thorough study of the rovibronic levels of BH$_2$, Kolbuszewski *et al.*[19] pointed out that "because of severe resonances in the excited electronic state, a very accurate potential energy surface will be needed for that state and for the ground state in order to obtain term values that agree precisely with the experimental results." These perturbations occur both between levels of the $\tilde{A}$ state and by Renner interactions

FIG. 7. Differences between calculated and observed energy levels of $^{11}BH_2$ (see Table I) for increasing levels of accuracy of the *ab initio* PESs. See the text for further explanations of the meaning of the various acronyms.

of excited state levels with nearby ground state levels. In particular, the authors found that the calculated $\tilde{A}$ state (0,10,0) and (0,12,0) Π levels of the various BH$_2$ isotopologues differed from experiment[15] by 26–43 cm^{-1} due to such resonances. By this criterion, the potential energy surfaces obtained in the present work must be very accurate indeed, as these differences between theory and experiment have been reduced to a matter of a few cm^{-1}. Furthermore, the sensitivity of the LIF experiments has allowed us to identify transitions to three perturbed ground state levels [(0,13,0) of $^{11}BH_2$ and $^{10}BH_2$ and (0,16,0) of $^{11}BD_2$] whose locations are precisely pinpointed by the calculations. The present data probe regions of the excited state potential of $^{11}BH_2$ from 11 717 cm^{-1} to 21 000 cm^{-1}, more than 9200 cm^{-1}, spanning ten bending levels and the five stretch-bend combination levels from (1,10,0) to (1,14,0). It is very gratifying that the calculated energy levels are in excellent agreement with experiment throughout this whole range (Table I and Fig. 7), illustrating once again the power of very high level *ab initio* theory to provide very reliable potential energy surfaces.

VI. CONCLUSIONS

In the present work, the LIF spectra of BH$_2$ and its various isotopologues have been obtained for the first time. These data have greatly expanded the range of observed excited state vibronic energy levels, from five bending levels of $^{11}BH_2$ in the pioneering work of Herzberg and Johns[15] to 15 in the present work, including ten bending levels and five stretch-bend combinations. We have also observed many more levels of $^{10}BH_2$, $^{11}BD_2$, and $^{10}BD_2$, yielding a very comprehensive data set for testing the results of our very high level *ab initio* calculations of the potential energy surfaces and variational prediction of the rovibronic energy levels. High resolution studies of the spectrum of $^{11}BD_2$ allowed us to determine of the ground state r_0 structure of BH$_2$ as r(BH) = 1.197(2) Å, θ = 129.6(2)°.

In order to predict the excited state energy levels to an accuracy within a few cm^{-1}, it was found necessary to include corrections for core correlation, extrapolation to the complete basis set limit, electron correlation beyond CCSD(T),
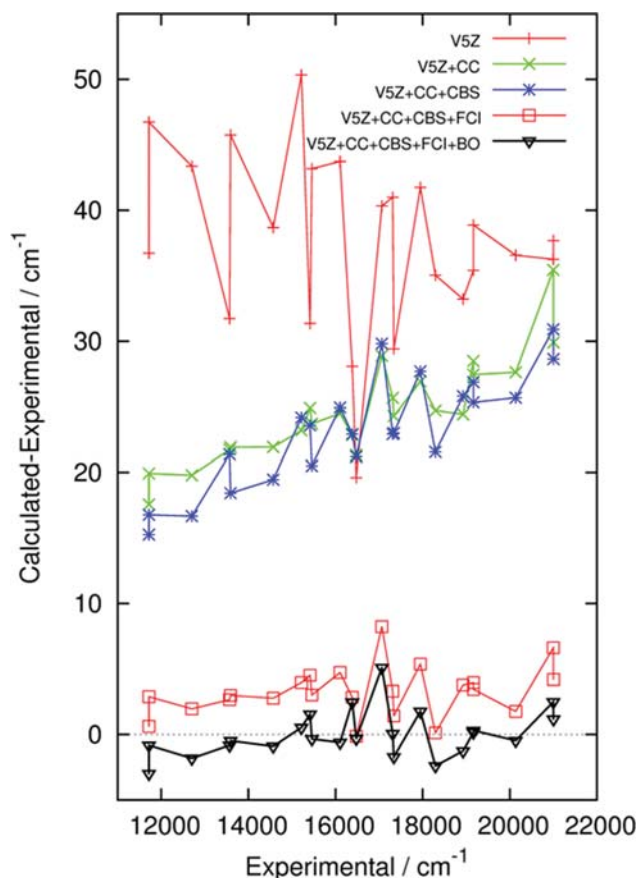
and diagonal Born-Oppenheimer effects to the original CCSD(T)/aug-cc-pV5Z potential energies. The resulting potentials, without any empirical adjustment or fitting to experimental data, gave excellent agreement with experiment, including perturbed levels and even allowed the assignment of a few transitions to high vibrational levels of the ground state that gained intensity by Renner-Teller mixing with the excited state.

ACKNOWLEDGMENTS

[1]A. O. Sezer and J. I. Brand, Mater. Sci. Eng., B **79**, 191-202 (2001).

[2]C. B. Samantaray and R. N. Singh, Int. Mater. Rev. **50**, 313 (2005).

[3]*Chemical Vapor Deposition. Principles Applications*, edited by M. L. Hitchman and K. F. Jensen (Academic Press, London, 1993).

[4]M. Sugawara, *Plasma Etching: Fundamentals and Applications* (Oxford University Press, Oxford, 1998).

[5]H. O. Pierson and A. W. Mullendore, Thin Solid Films **83**, 87 (1981).

[6]W. Fichtl, Mater. Des. **2**, 276 (1981).

[7]S.-G. He, D. J. Clouthier, A. G. Adam, and D. W. Tokaryk, J. Chem. Phys. **122**, 194314 (2005), and references therein.

[8]S.-G. He, F. X. Sunahori, and D. J. Clouthier, J. Am. Chem. Soc. **127**, 10814 (2005).

[9]F. X. Sunahori, D. J. Clouthier, S. Carter, and R. Tarroni, J. Chem. Phys. **130**, 164309 (2009).

[10]F. X. Sunahori and D. J. Clouthier, J. Chem. Phys. **130**, 164310 (2009).

[11]R. Tarroni and D. J. Clouthier, J. Chem. Phys. **133**, 064304 (2010).

[12]J. Yang and D. J. Clouthier, J. Chem. Phys. **135**, 094305 (2011).

[13]R. Grimminger, P. M. Sheridan, and D. J. Clouthier, J. Chem. Phys. **140**, 164302 (2014).

[14]M. A. Gharaibeh, R. Nagarajan, D. J. Clouthier, and R. Tarroni, J. Chem. Phys. **142**, 014305 (2015).

[15]G. Herzberg and J. W. C. Johns, Proc. R. Soc. A **298**, 142 (1967).

[16]L. B. Knight, M. Winiski, P. Miller, C. A. Arrington, and D. Feller, J. Chem. Phys. **91**, 4468 (1989).

[17]M. Peric, S. D. Peyerimhoff, and R. J. Buenker, Can. J. Chem. **59**, 1318 (1981).

[18]M. Brommer, P. Rosmus, S. Carter, and N. C. Handy, Mol. Phys. **77**, 549 (1992).

[19]M. Kolbuszewski, P. R. Bunker, W. P. Kraemer, G. Osmann, and P. Jensen, Mol. Phys. **88**, 105 (1996).

[20]P. R. Rablen and J. F. Hartwig, J. Am. Chem. Soc. **118**, 4648 (1996).

[21]Y. Liu, K. Su, Q. Zeng, L. Cheng, and L. Zhang, Struct. Chem. **23**, 1677 (2012).

[22]K. Sato, N. Kanda, T. Ogata, and Y. Kumashiro, Chem. Phys. Lett. **325**, 453 (2000).

[23]D. Feller, D. A. Dixon, and K. A. Peterson, J. Phys. Chem. A **102**, 7053 (1998).

[24]K. Sato and Y. Kubota, Appl. Phys. Express **4**, 056202 (2011).

[25]M. D. Allendorf and C. F. Melius, J. Phys. Chem. A **101**, 2670 (1997).

[26]D. C. Miller, J. J. O'Brien, and G. H. Atkinson, J. Appl. Phys. **65**, 2645 (1989).

[27]H. Harjanto, W. W. Harper, and D. J. Clouthier, J. Chem. Phys. **105**, 10189 (1996).

[28]D. L. Michalopoulos, M. E. Geusic, P. R. R. Langridge-Smith, and R. E. Smalley, J. Chem. Phys. **80**, 3556 (1984).

[29]S. Gerstenkorn and P. Luc, Atlas Du Spectre D'absorption de la Molécule D'iode (Editions du C.N.R.S., Paris, 1978); Rev. Phys. Appl. **14**, 791 (1979).

[30]A. Word and J. Ruff, in *Inorganic Syntheses* (McGraw Hill, New York, 1973), Vol. 11, p. 15.

[31]K. Dressler and D. A. Ramsey, Philos. Trans. R. Soc., A **251**, 553 (1959).

[32]J. A. Pople and H. C. Longuet-Higgins, Mol. Phys. **1**, 372 (1958).

[33]See supplementary material at http://dx.doi.org/10.1063/1.4919094 for tables including all of the assigned LIF transitions and the coefficients obtained from fitting the *ab initio* potential energy surfaces.

[34]R. A. Kendall, T. H. Dunning, Jr., and R. J. Harrison, J. Chem. Phys. **96**, 6796 (1992).

[35]K. Raghavachari, G. W. Trucks, J. A. Pople, and M. Head-Gordon, Chem. Phys. Lett. **157**, 479 (1989).

[36]K. A. Peterson and T. H. Dunning, Jr., J. Chem. Phys. **117**, 10548 (2002).

[37]D. W. Schwenke, J. Chem. Phys. **122**, 014107 (2005).

[38]P. J. Knowles and N. C. Handy, Chem. Phys. Lett. **111**, 315 (1984); Comput. Phys. Commun. **54**, 75 (1989).

[39]N. C. Handy, J. Yamaguchi, and H. F. Schaefer, J. Chem. Phys. **84**, 4481 (1986).

[40]S. Carter, N. C. Handy, P. Rosmus, and G. Chambaud, Mol. Phys. **71**, 605 (1990).

[41]M. Brommer, B. Weis, B. Follmeg, P. Rosmus, S. Carter, N. C. Handy, H.-J. Werner, and P. J. Knowles, J. Chem. Phys. **98**, 5222 (1993).

[42]M. Brommer, Ph.D. thesis, Johann Wolfgang Goethe Universität, Frankfurt am Main, Germany, 1993.

[43]CFOUR, a quantum-chemical program package by J. F. Stanton, J. Gauss, M. E. Harding, and P. G. Szalay with contributions from A. A. Auer, R. J. Bartlett, U. Benedikt, C. Berger, D. E. Bernholdt, Y. J. Bomble, L. Cheng, O. Christiansen, M. Heckert, O. Heun, C. Huber, T.-C. Jagau, D. Jonsson, J. Jusélius, K. Klein, W. J. Lauderdale, D. A. Matthews, T. Metzroth, L. A. Mück, D. P. O'Neill, D. R. Price, E. Prochnow, C. Puzzarini, K. Ruud, F. Schiffmann, W. Schwalbach, S. Stopkowicz, A. Tajti, J. Vázquez, F. Wang, and J. D. Watts and the integral packages MOLECULE (J. Almlöf and P. R. Taylor), PROPS (P. R. Taylor), ABACUS (T. Helgaker, H. J. Aa. Jensen, P. Jørgensen, and J. Olsen), and ECP routines by A. V. Mitin and C. van Wüllen. For the current version, see http://www.cfour.de.

[44]H.-J. Werner, P. J. Knowles, F. R. Manby, M. Schütz, P. Celani, G. Knizia, T. Korona, R. Lindh, A. Mitrushenkov, G. Rauhut, T. B. Adler, R. D. Amos, A. Bernhardsson, A. Berning, D. L. Cooper, M. J. O. Deegan, A. J. Dobbyn, F. Eckert, E. Goll, C. Hampel, A. Hesselmann, G. Hetzer, T. Hrenar, G. Jansen, C. Köppl, Y. Liu, A. W. Lloyd, R. A. Mata, A. J. May, S. J. McNicholas, W. Meyer, M. E. Mura, A. Nicklass, P. Palmieri, K. Pflüger, R. Pitzer, M. Reiher, T. Shiozaki, H. Stoll, A. J. Stone, R. Tarroni, T. Thorsteinsson, M. Wang, and A. Wolf, MOLPRO, version 2010.1, a package of *ab initio* programs, 2010, see http://www.molpro.net.

[45]J. Senekowitsch, Ph.D. thesis, Johann Wolfgang Goethe Universität, Frankfurt am Main, Germany, 1988.

[46]S. Carter, N. C. Handy, C. Puzzarini, R. Tarroni, and P. Palmieri, Mol. Phys. **98**, 1697 (2000).

[47]A. O. Mitrushchenkov, J. Chem. Phys. **136**, 024108 (2012).

[48]F. X. Sunahori and D. J. Clouthier, J. Chem. Phys. **130**, 164310 (2009).

[49]F. S. Pianalto, L. C. O'Brien, P. C. Keller, and P. F. Bernath, J. Mol. Spectrosc. **129**, 348 (1988).

[50]K. Kawaguchi, J. Chem. Phys. **96**, 3411 (1992).

[51]O. L. Polyansky, R. I. Ovsyannikov, A. A. Kyuberis, L. Lodi, J. Tennyson, and N. F. Zobov, J. Phys. Chem. A **117**, 9633 (2013).